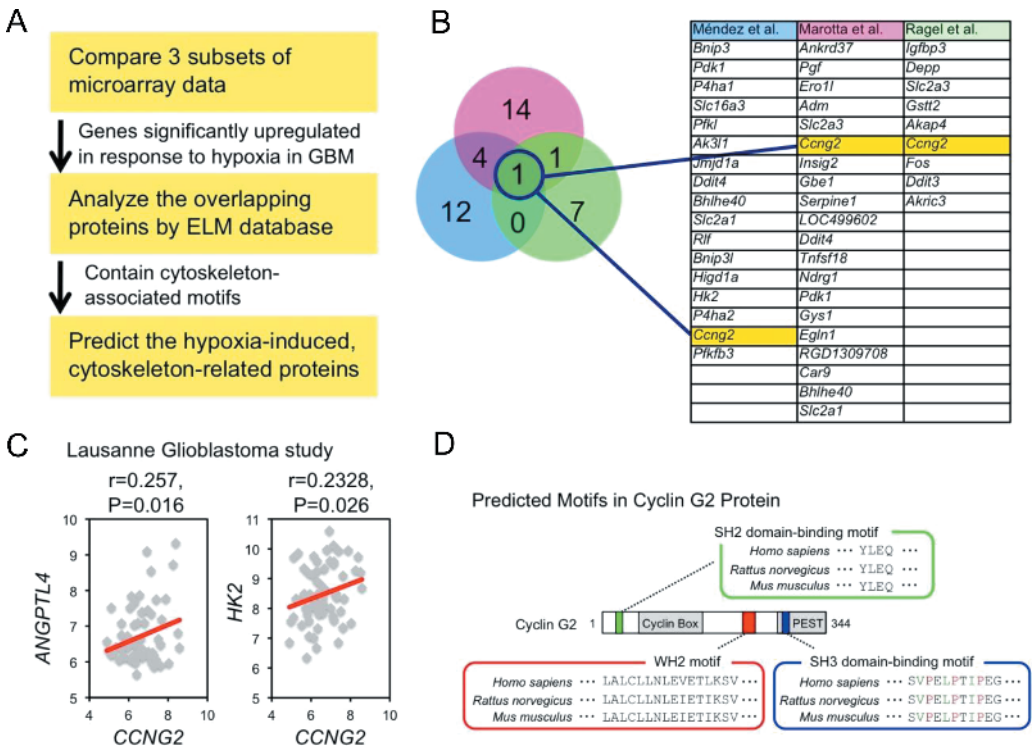

Figure W1. (A) Diagram of the procedure to predict the hypoxia-induced and cytoskeleton-associated proteins in human glioma cell lines. (B) *Cyclin G2* is a commonly upregulated gene in response to hypoxia among three subsets of microarray data of glioblastoma study. (C) The expression level of cyclin G2 is correlated with hypoxia-responsive genes, *ANGPTL4* and *HK2*, in Lausanne glioblastoma study (Accession ID: GSE7696). (D) The ELM database predicts that cyclin G2 protein has a putative SH2 or SH3 domain–binding motif and WH2 motif.

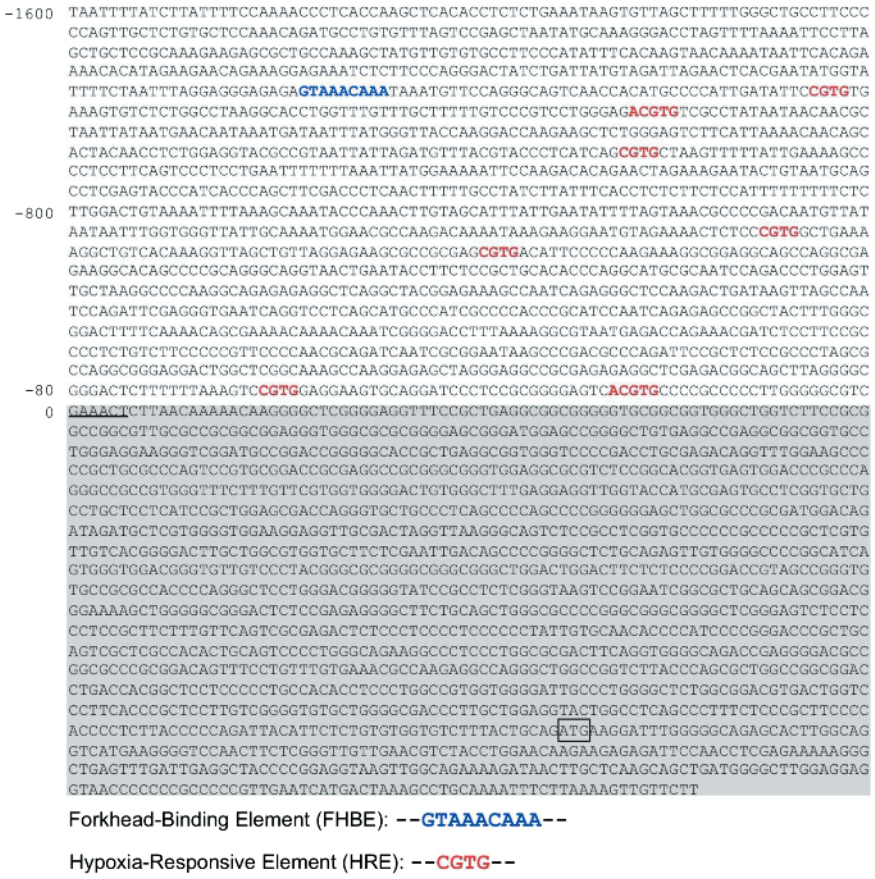

Figure W2. The human cyclin G2 promoter region contains putative HREs. The human cyclin G2 promoter region (−1600~0) contains some putative HREs (-CGTG-; red) and a FoxO3a-binding site (blue). The transcription starting site (underlined in shaded sequence) and the translation initiating ATG (boxed) were determined according to NCBI (Accession No. NM_004354.2).

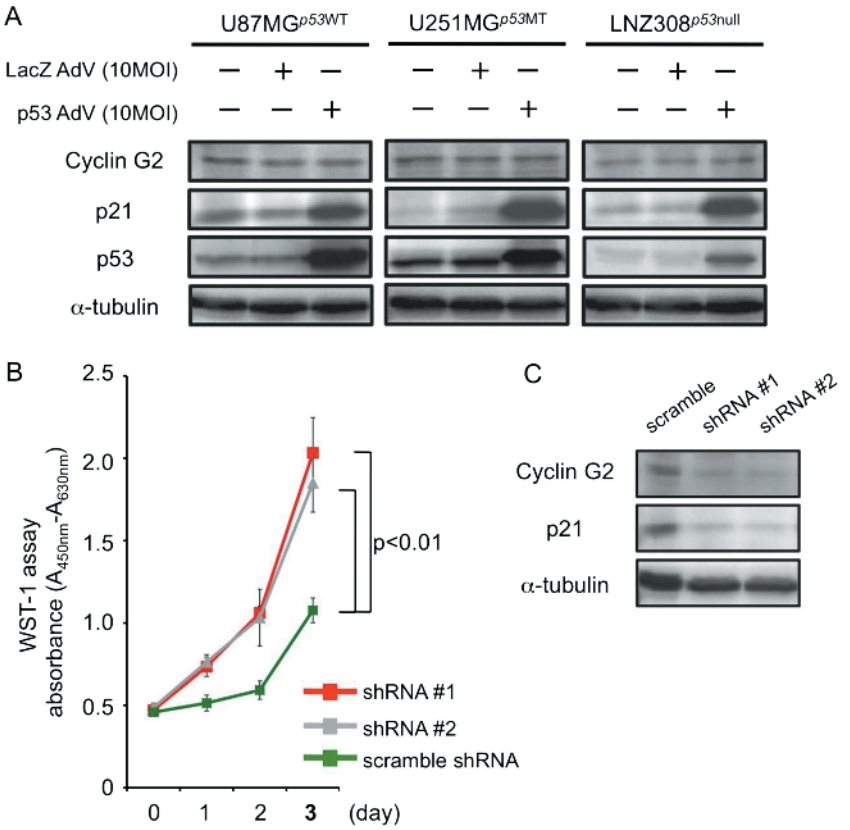

Figure W3. (A) Western blot analyses of U87MG (p53^{WT}), U251MG (p53^{Mut}), and LNZ308 (p53^{Null}) cells infected with *lacZ* or p53 adenovirus. These results show that the level of p53 does not affect that of cyclin G2 and forced expression of p53 does not induce cyclin G2 expression in GBM. (B) WST-1 assay showing the effect of cyclin G2's reduction on cell-cycle regulation in U87MG cells. (C) Cyclin G2 reduction resulted in p21 suppression.

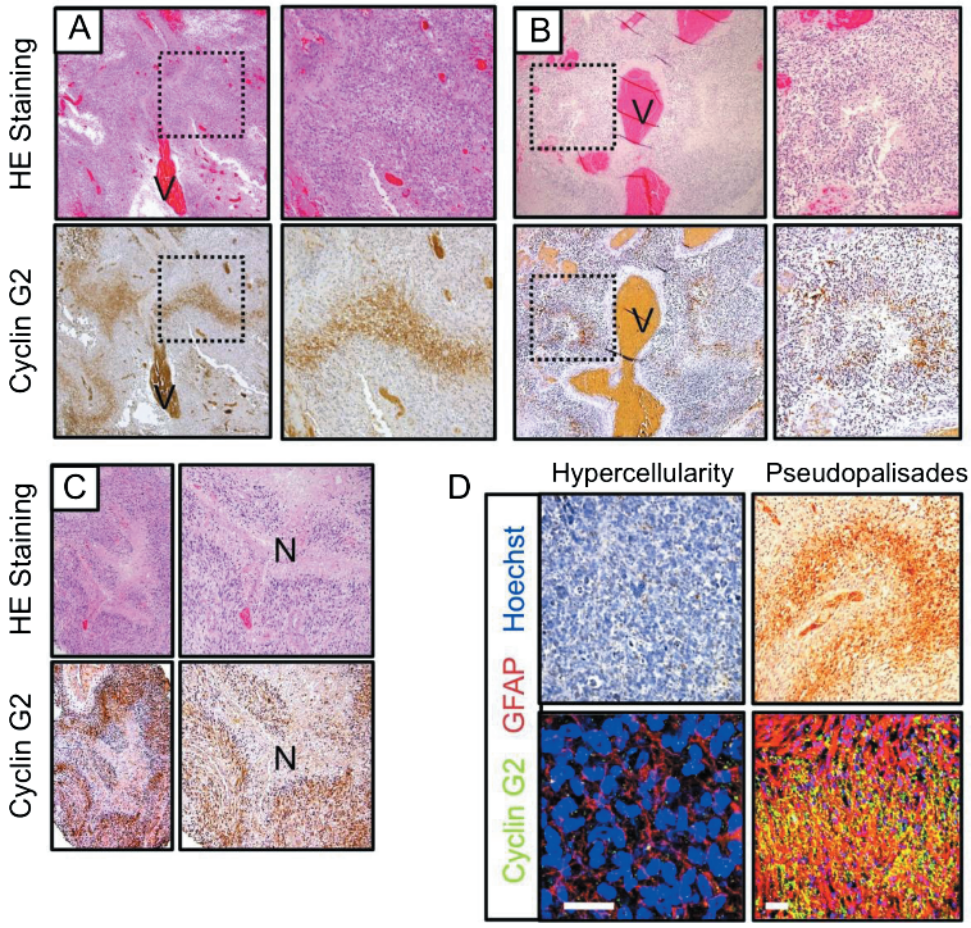

Figure W4. Cyclin G2 is abundant in pseudopalisade-forming glioma cells. (A–C) Cyclin G2 expression in pseudopalisades is observed in various types of GBM specimens. (D) Cyclin G2 is absent in high cellularity/high mitotic regions in GBM. The scale bars represent 10 μm in D. "V" and "N" indicate vessel and necrosis, respectively.

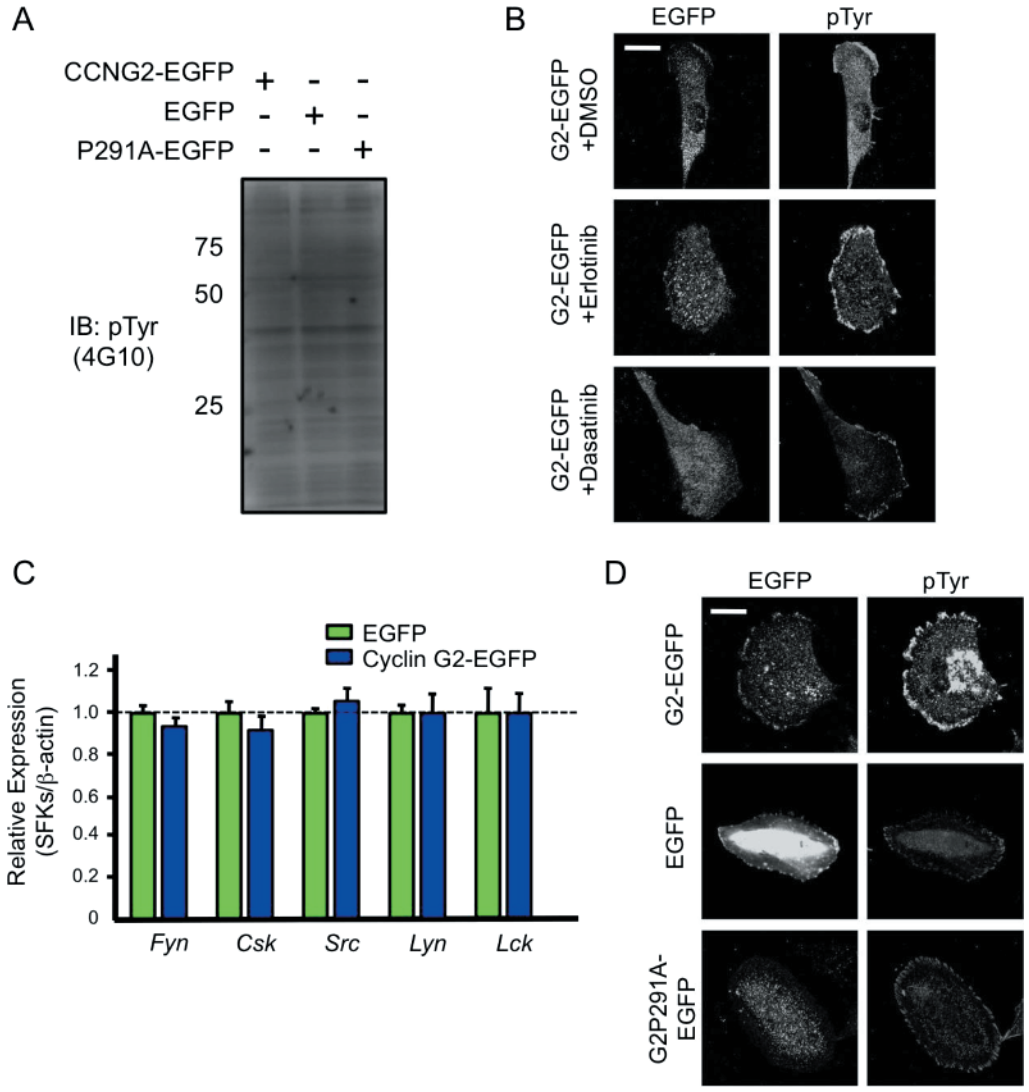

Figure W5. Cyclin G2 induces the restricted tyrosine phosphorylation of cortactin in an SFK-dependent manner. (A) Ectopic expression of cyclin G2 does not alter the total amount of tyrosine phosphorylation. (B) Dasatinib inhibits the phosphorylation induced by cyclin G2. Note that dasatinib, but not erlotinib, decreases the peripheral signals of phosphotyrosine induced by cyclin G2. The scale bar represents 10 μm in B. (C) Cyclin G2 does not enhance transcription of SFK mRNA. (D) Exogenous cyclin G2 increases, whereas the P291A mutant impairs, tyrosine phosphorylation signals at the juxtamembrane. The scale bar represents 10 μm in D.

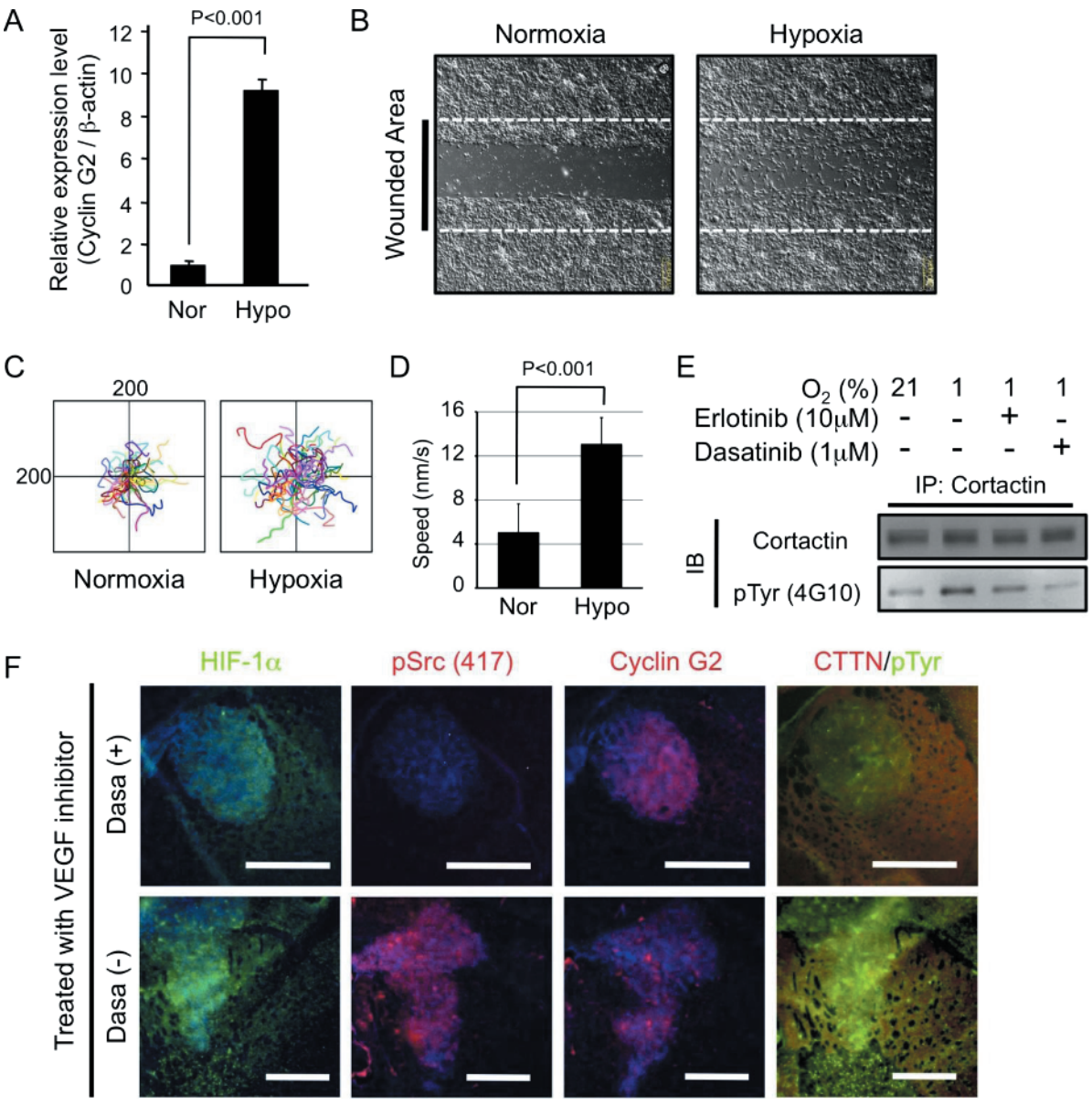

Figure W6. The effectiveness of dasatinib on the expansion of glioma-initiating cells. (A) Cyclin G2 expression is enhanced in response to hypoxia in murine glioma-initiating 005 cells. (B–D) Hypoxia stimulates the motility of 005 cells. (E) Tyrosine phosphorylation of cortactin is enhanced in response to hypoxic stimulation in 005 cells and dasatinib attenuates it. Note that 005 cells show the phosphorylation in a normoxic and steady state. (F) Dasatinib attenuates the hypoxia-driven local invasion of 005 cells. Note that dasatinib treatment inhibits the phosphorylation of src and cortactin. The scale bars represent 200 μm (F).

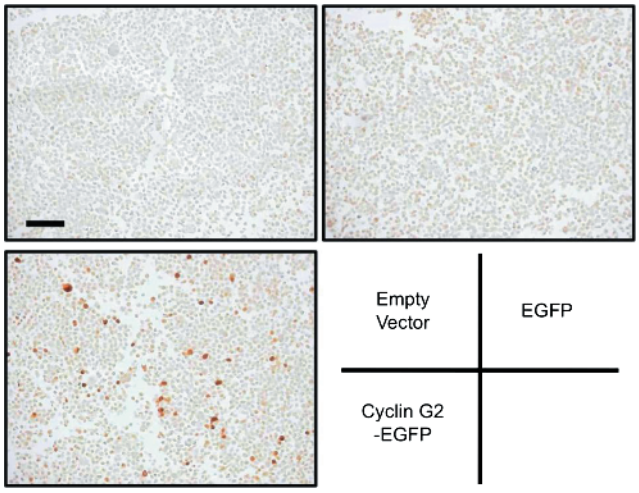

Figure W7. Goat anti-human cyclin G2 antibody (Santa Cruz Biotechnology, Inc) successfully recognized ectopic cyclin G2 in paraffin-embedded HEK293 cells that were transfected with cyclin G2–EGFP. For other applications including immunoblot analysis, see references. The scale bar represents 100 μm.

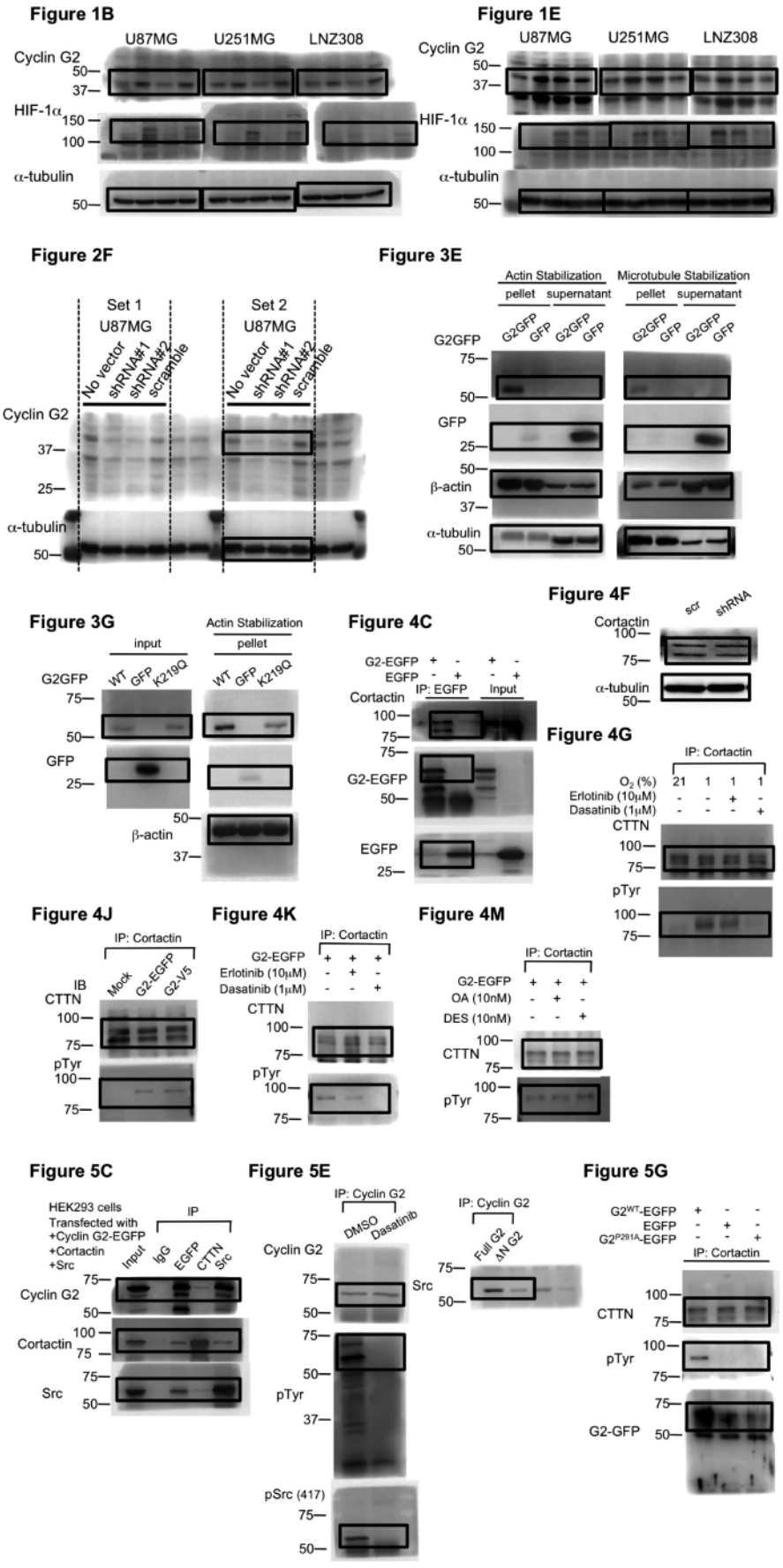

Figure W8. Full scans of the immunoblots shown in the figures. Boxes indicate the parts used in the figures, and numbers indicate the molecular weights. All data were obtained with the VersaDoc Imaging System (Bio-Rad).